

Zero-P-to-3: Zero-Shot Partial-View Images to 3D Object

Yuxuan Lin¹ Ruihang Chu¹ Zhenyu Chen² Xiao Tang² Lei Ke¹ Haoling Li¹
Yingji Zhong³ Zhihao Li² Shiyong Liu² Xiaofei Wu² Jianzhuang Liu² Yujiu Yang¹

¹Tsinghua University

²Huawei Technologies Co., Ltd.

³The Hong Kong University of Science and Technology

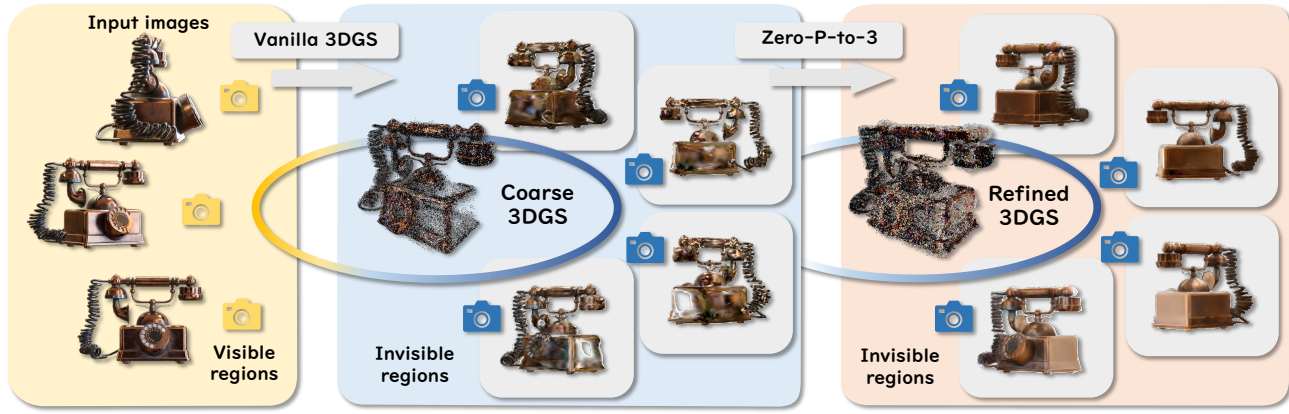


Figure 1. Zero-P-to-3 reconstructs 3D objects where visible regions are confined to a limited field-of-view. We first reconstruct a coarse 3D Gaussian Splatting (3DGS) model from partial observations, then iteratively refine it using multiple priors to obtain the final 3DGS model.

Abstract

Generative 3D reconstruction shows strong potential in incomplete observations. While sparse-view and single-image reconstruction are well-researched, partial observation remains underexplored. In this context, dense views are accessible only from a specific angular range, with other perspectives remaining inaccessible. This task presents two main challenges: (i) limited View Range: observations confined to a narrow angular scope prevent effective traditional interpolation techniques that require evenly distributed perspectives. (ii) inconsistent Generation: views created for invisible regions often lack coherence with both visible regions and each other, compromising reconstruction consistency. To address these challenges, we propose Zero-P-to-3, a novel training-free approach that integrates the local dense observations and multi-source priors for reconstruction. Our method introduces a fusion-based strategy to effectively align these priors in DDIM sampling, thereby generating multi-view consistent images to supervise invisible views. We further design an iterative refinement strategy, which uses the geometric structures of the object to enhance reconstruction quality. Extensive experiments on multiple

datasets show the superiority of our method over SOTAs, especially in invisible regions.

1. Introduction

The field of 3D object reconstruction has witnessed significant evolution in recent years. This task aims to reconstruct the geometry and texture of objects from available observations. As complete observations are not always accessible due to occlusions or constraints in camera positioning, generative models leveraging prior knowledge have emerged as promising solutions. While existing approaches [12, 16, 17, 32–34, 38, 39], especially with diffusion models [21], have made considerable progress, they mainly focus on reconstruction from a single image [12, 16, 17, 32] or well-spaced sparse views [1, 33, 34, 38, 39]. Yet, partial observation scenarios are more common in daily life, where dense object observations are available from certain views but inaccessible from other angles. For instance, in cluttered indoor environments, objects can be partially occluded by furniture or walls, making it difficult to capture all of their views.

3D reconstruction from a restricted range of observation angles presents unique characteristics and challenges. Compared to single-image reconstruction, this setting provides

dense observations over certain regions, offering more local information that has the potential to achieve high-quality reconstruction results. However, effectively combining these partial views to infer better structures remains underexplored. It differs from sparse-view reconstructions as well. Generally, these sparse views are often evenly distributed around the object and provide broader coverage [38], but partial observations confined to a limited range may leave substantial portions of the object completely unseen. As a result, traditional interpolation methods [1, 18, 34, 38, 42] used in sparse-view reconstruction are not applicable.

Current generative reconstruction approaches may face critical challenges in partial observation scenarios. Most multi-view diffusion methods [12, 15–17, 24, 32] only take a single image as input to generate a fixed set of novel views. These generated views often exhibit inconsistencies both with the ground truth and among each other, preventing reliable supervision for reconstruction. Even advanced approaches that support multi-image inputs, such as LEAP [8] and EscherNet [11], continue to struggle with coherent generation quality. This challenge arises because the 3D features corresponding to multiple inputs are not perfectly aligned, leading to inconsistencies in the generated content. Similarly, methods like Trellis [35] that generate 3D content directly from latent 3D representations cannot guarantee consistency between the generated content and visible information, as the 3D latent space often fails to preserve the detailed information present in the input images. When applied to partial observation settings, these generation paradigms lack effective mechanisms to collectively utilize dense information from visible image sets. In contrast, neural reconstruction repair methods [33, 34, 38, 39] operate by refining existing Gaussian representations. While these methods can effectively utilize information from visible regions, they leverage local information from other sparse views to enhance image features. Unlike the multi-view diffusion approaches, these repair mechanisms rely heavily on surrounding views for effective feature propagation, making them suitable when observations are well-distributed around 360° , but less effective in partial observation settings where large regions remain completely invisible.

To address these challenges, we introduce a novel **Zero**-shot approach to transfer Partial-view image observations **to** reconstructed 3D object, termed as Zero-P-to-3. It is a training-free framework that integrates multiple priors and conditions for effective 3D reconstruction from partial observation. As illustrated in Fig. 1, Zero-P-to-3 begins by constructing a coarse 3D Gaussian Splatting model (3DGS) [9] using the available dense observations from views within a specific angular range. Building upon this initial reconstruction, we propose a fusion-based strategy that aligns various priors and conditions in the diffusion-

based inference stage. Specifically, our method integrates information from multiple viewing angles, rendering results, multi-view diffusion priors, and image restoration priors into each denoising timestep. This fusion process generates a batch of high-quality, consistent images in novel views as the supervision, guiding the subsequent reconstruction process.

To further enhance the reconstruction quality, we design an iterative refinement framework to utilize rotated view sampling. Given that our observations cover a local region, we propose to rotate supervision views around these observed areas, thereby maximizing view coverage to provide dense supervision signals. This design efficiently leverages information from visible regions and enhances multi-view consistency by utilizing geometric structures and weak textures of the object during the rotation process, finally mitigating reconstruction artifacts.

Our Zero-P-to-3 presents significant superiority for partial observation reconstruction. By leveraging multiple priors and supervision from rotated views, we preserve fine details in observed regions while maintaining consistency across novel viewpoints. Unlike methods that require additional training on extra datasets, our Zero-P-to-3 provides a training-free solution adaptable to diverse scenarios. Experimental evaluations on objects with front-facing observations demonstrate that Zero-P-to-3 achieves significantly higher consistency with original observations compared to existing approaches. Our method effectively handles challenging cases involving complex geometry and occlusions. Our main contributions are as follows:

- We investigate a practical yet challenging problem of 3D reconstruction from partial observations, and propose a novel training-free framework as a solution.
- We integrate multi-source priors with a rotated view refinement strategy to leverage local observations, enhancing the accuracy and detail of reconstruction.
- Extensive experiments show our method’s superiority in reconstruction quality and multi-view consistency.

2. Reated Work

3D Sparse Reconstruction. Traditional 3D sparse reconstruction methods primarily focus on scenarios with sparse but well-distributed viewpoints. RegNeRF [18] introduces color-based regularization terms, while DS-NeRF [3] leverages depth supervision for robust reconstruction under sparse views. LEAP [8] further addresses sparse-view 3D modeling by eliminating reliance on precise camera poses. CVT-xRF [42] and Binocular-Guided 3D Gaussian Splatting [5] advance this direction by modeling pixel relationships and view consistency through 3D Gaussian point cloud representations. Recent learning-based approaches show remarkable efficiency, with methods like LRM [7], LGM [27], and GRM [37] leveraging large-scale models

for efficient single-image or sparse-view reconstruction using transformer architectures. Generative models such as EscherNet [11] explore scalable view synthesis through diffusion-based frameworks, while Structured3D [35] introduces structured latent representations for versatile 3D generation. Similarly, Triplane Meets Gaussian Splatting [43], Splatter Image [26], and InstantMesh [36] focus on improving reconstruction speed while maintaining quality through various optimization techniques. Unlike these methods that rely on learned priors or training, our approach operates in a training-free manner while effectively handling partial dense observations.

Diffusion-Based Generation and Reconstruction. The integration of diffusion models has revolutionized 3D content generation and reconstruction. DreamFusion [19] pioneers text-to-3D generation using 2D diffusion models, with Magic3D [13] and Magic123 [20] improving efficiency and quality. SJC [30] proposes an alternative optimization approach to Score Distillation Sampling, offering improved stability in knowledge transfer from 2D to 3D. Zero123++ [23] and SyncDreamer [16] focus on generating consistent multi-view images from a single view. For reconstruction, ReconFusion [33] and DiffusionERF [34] enhance 3D reconstruction using 2D image priors from diffusion models. GaussianObject [38] achieves high-quality reconstruction from extremely limited views. LM-Gaussian [39] introduces large-scale visual model priors for sparse-view reconstruction with robust initialization. Multi-view diffusion approaches like ViewCrafter [40], DimVis [4], ReconX [14], and ViewDiff [6] demonstrate consistent multi-view image generation for 3D reconstruction. Recent approaches including MVDream [24], Wonder3D [17], SV3D [29], and Era3D [12] further improves generation quality and efficiency. While these methods typically reconstruct or generate from a single image or images covering the entire scene, whereas our approach uniquely combines diffusion priors with geometric constraints to handle partial dense observations.

3. Method

3.1. Task Definition

Our work addresses the challenge of novel view synthesis from spatially constrained observations. Given a set of N images $\mathbf{X}_{\text{ref}} = \{x_i\}_{i=1}^N$ captured from a limited spatial region (e.g., approximately 90°), we aim to construct a high-quality 3D Gaussian Splatting (3DGS) model \mathcal{G} capable of generating photorealistic renderings from arbitrary viewpoints. As shown in Fig. 2, these images are taken within a segment of a sphere, with each input image accompanied by its corresponding object mask m_i generated by SAM, collectively represented as $\mathbf{M}_{\text{ref}} = \{m_i\}_{i=1}^N$.

Our aim is to learn a function that generates new views



Figure 2. Visualizations of input images (top), masks (middle), and processed images (bottom) from the RefNeRF [28] dataset.

based on arbitrary camera poses π , denoted as $x = \mathcal{G}(\pi | \{x_i, \pi_i, m_i\}_{i=1}^N)$. This challenging task requires addressing several key issues: establishing accurate geometric foundations from partial observations, generating high-quality and consistent images for invisible regions, and ensuring globally consistent optimization. Our approach, illustrated in Fig. 3, consists of three key stages: (1) coarse 3DGS initialization from partial observations, (2) multi-prior score fusion for view-consistent image generation, and (3) iterative refinement through rotated view sampling.

3.2. Coarse Gaussians Initialization

To initialize the 3DGS model, we first estimate the camera intrinsics \mathbf{K}_{ref} and extrinsics $\Pi_{\text{ref}} = \{\pi_i\}_{i=1}^N$ for the input images \mathbf{X}_{ref} using Structure From Motion (SFM) techniques [22]. Leveraging these parameters, we construct an initial coarse 3DGS model $\mathcal{G}_0 = \{g_j\}_{j=1}^M$, where each Gaussian g_j is parameterized by a 3D position \mathbf{p}_j , a covariance matrix Σ_j defining its spatial extent, an opacity α_j , and spherical harmonics coefficients \mathbf{Y}_j for view-dependent color. The initialization is optimized by minimizing the photometric reconstruction error over visible regions across all input images:

$$\mathcal{G}_0 = \arg \min_{\mathcal{G}} \sum_{i=1}^N \sum_{\mathbf{p}_j \in \mathcal{V}_i} \|\mathcal{R}(\mathbf{p}_j, \Sigma_j, \alpha_j, \mathbf{Y}_j, \pi_i) - x_i(\mathbf{p}_j)\|^2, \quad (1)$$

where \mathcal{V}_i represents the set of 3D points visible in image x_i , and $\mathcal{R}(\cdot)$ denotes the volumetric rendering function of the 3DGS model. To enhance robustness, we incorporate the object masks m_i to focus optimization on the foreground object, reducing interference from background noise. While \mathcal{G}_0 effectively captures the coarse geometry and appearance of visible areas, it typically exhibits incomplete details and inconsistencies in occluded or unseen regions, which necessitates a subsequent refinement stage.

3.3. Multi-Prior Score Fusion

To synthesize consistent, high-quality images for novel views, particularly in invisible regions, we propose a diffusion-based strategy termed Multi-Prior Score Fusion. Diffusion models generate images by iteratively estimat-

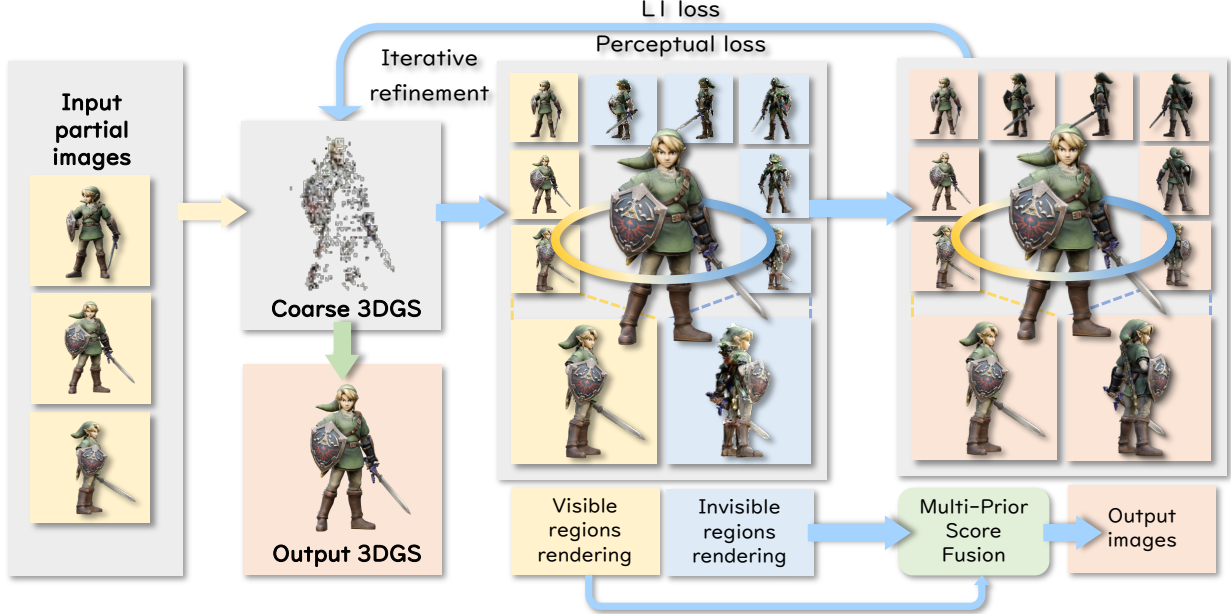


Figure 3. Overview of Zero-P-to-3 for 3D reconstruction from partial observations. Starting with input partial images, the system first constructs a coarse 3D Gaussian Splatting (3DGS) model, then renders both visible and invisible regions. These renderings are enhanced through Multi-Prior Score Fusion to generate high-quality output images that serve as supervision for refining the 3DGS model. Through iterative refinement using L1 and perceptual losses, the system produces a comprehensive 3D representation that effectively bridges the gap between limited observations and complete object reconstruction.

ing the score function $\nabla_x \log p(x_t)$, progressively denoising from pure noise ($t = 1$) to a clean image ($t = 0$). Our goal is to synthesize a target view x_t conditioned on a set of reference views $\{V_i\}_{i=1}^N$, extending multi-view diffusion (MVD) from a single-input to a multi-input framework. A simple approach to ensure consistency across inferences from different reference views is to average the individual view-conditioned scores:

$$\nabla_x \log p(x_t | \{V_i\}_{i=1}^N) \approx \frac{1}{N} \sum_{i=1}^N \nabla_x \log p(x_t | V_i), \quad (2)$$

where x_t is the target view at diffusion step t , $\{V_i\}_{i=1}^N$ is the set of N reference views, and $\nabla_x \log p(x_t | \cdot)$ denotes the log-probability gradient of x_t conditioned on the respective views. This approximation combines gradient information from each reference view, guiding the synthesis of x_t toward a solution consistent with all inputs. By averaging, the method aligns inferences by assuming each view contributes equally to a unified representation of the target.

However, this approach has limitations. It assumes that each view contributes equally to the target view, though this varies significantly with the angle between them. More critically, it implies conditional independence among reference views, expressed as $p(x_t | \{V_i\}) \propto \prod_{i=1}^N p(x_t | \{V_i\}_{i=1}^N)$, since the averaged score in Eq. 2 reflects a product form when summing log-probabilities. In practice, such independence rarely holds due to correlated scene details across

views, resulting in artifacts like blurriness in unobserved regions (see Fig. 11). We address this limitation through robust geometric and texture regularization, overcoming the theoretical flaws of the multi-view fusion approximation.

3.3.1. Multi-View Fusion

In our implementation, we use a standard multi-view diffusion (MVD) framework:

$$\varepsilon_{\text{MVD}}(x_t) = \sum_{i=1}^N w_i \cdot \varepsilon_{\text{MVD}}(x_t | V_i), \quad (3)$$

where $\varepsilon_{\text{MVD}}(x_t | V_i)$ represents the noise predicted by a diffusion model conditioned on view V_i , and w_i denotes the weight. For the weight configuration, frontal views are assigned a weight of 2, back views receive 1.5, and other viewpoints are allocated a weight of 1. In spite of this, the core challenge stems from correlations between views that invalidate the independence assumption, requiring a more substantive solution.

3.3.2. Frequency-Decomposed Regularization

The key contribution of our approach is the integration of complementary priors that operate across different frequency bands, effectively regularizing against the invalid independence assumption in multi-view fusion. We incorporate two critical regularizing components:

(i) Geometric Rendering prior Derived from the initial 3DGS model \mathcal{G}_0 , this prior provides essential low-frequency

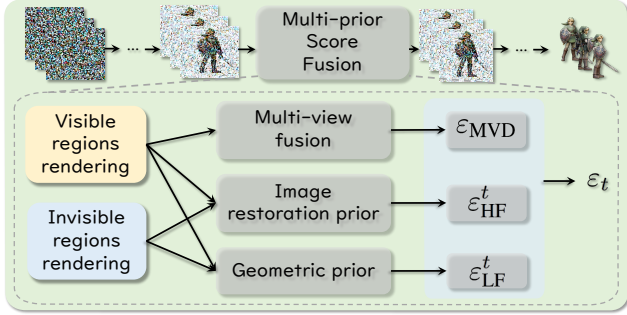


Figure 4. The Multi-Prior Score Fusion framework combines three components to generate novel view images: multi-view diffusion (ε_{MVD}) for fusing reference view information, geometric prior (ε_{LF}^t) for structural consistency, and image restoration prior (ε_{HF}^t) for enhancing details. These components process both visible and invisible regions from reference views and are combined with time-dependent weights to produce the noise prediction ε_t used in DDIM sampling for the final image generation.

(LF) structural regularization. It generates a coarse rendering x_{LF} at the target viewpoint, with noise prediction:

$$\varepsilon_{LF}^t = \frac{x_t - \sqrt{\alpha_t} x_{LF}}{\sqrt{1 - \alpha_t}}, \quad (4)$$

where ε_{LF}^t is the low-frequency noise prediction at timestep t , x_t is the noisy image at timestep t , α_t is the noise schedule parameter, and x_{LF} is the coarse rendering result. This structural prior directly addresses the limitations of the multi-view approximation by enforcing global geometric consistency independent of reference views. Rather than relying on potentially correlated view information, it provides an orthogonal, geometry-based regularization that stabilizes the generation process, particularly in regions where view correlation issues are most problematic.

(ii) Image Restoration prior This complements the geometric guidance by enhancing high-frequency (HF) features such as textures and edges. This texture-focused prior generates noise predictions ε_{HF}^t that refine local details, which are often inadequately captured by either the geometric prior or the multi-view fusion. By focusing on textures and fine details, this prior further mitigates the effects of the invalid independence assumption by introducing information beyond what is captured in the potentially correlated views.

We combine these regularizing priors with the MVD framework using time-dependent weights that align with the diffusion process:

$$\varepsilon_t = \varepsilon_{MVD} + w_{HF}(t)\varepsilon_{HF}^t + w_{LF}(t)\varepsilon_{LF}^t, \quad (5)$$

where ε_t is the combined noise prediction, ε_{MVD} is the base multi-view diffusion noise prediction, $w_{HF}(t)$ and $w_{LF}(t)$ are time-dependent weights, and ε_{HF}^t and ε_{LF}^t are the high-frequency and low-frequency noise predictions, respectively.

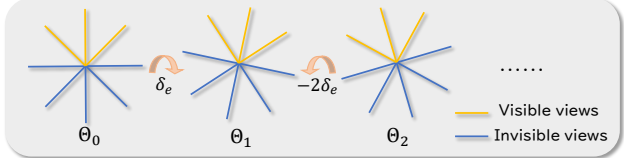


Figure 5. Schematic diagram of rotated views. Yellow lines indicate visible views used as conditional inputs for fusion-based inference, while blue lines represent invisible views that provide geometric and coarse texture information requiring restoration. Starting from initial angle Θ_0 , viewpoints are rotated in batches of N to angles Θ_1 , Θ_2 , etc., progressively densifying the viewpoints until complete dense supervision of the object is achieved.

tively. The weights follow a smooth transition schedule:

$$w_{LF}(t) = \frac{\tanh(-(t - \tau)/\sigma) + 1}{2}, \quad w_{HF}(t) = \frac{1 - w_{LF}(t)}{\eta}, \quad (6)$$

where τ controls the transition point, σ determines the smoothness, and η scales the high-frequency weight. These parameters govern the shift from low to high-frequency regularization during diffusion, ensuring geometric structure dominates at large t while texture refinement becomes prominent at small t .

By introducing geometric and texture priors that operate orthogonally to the multi-view conditioning, we effectively compensate for the invalid independence assumption inherent in standard multi-view fusion. The geometric prior provides structural coherence that counteracts the correlation-induced artifacts, while the texture prior enhances details that might be lost or blurred.

3.3.3. Sampling Process

We integrate the regularized noise prediction ε_t into the Denoising Diffusion Implicit Model (DDIM) sampling:

$$x_{t-1} = x_t + (\sqrt{\alpha_{t-1}} - \sqrt{\alpha_t}) \frac{\varepsilon_t}{\sqrt{1 - \alpha_t}}. \quad (7)$$

This efficient sampling approach enables the generation of high-quality novel views, even for viewpoints significantly distant from the observed views.

As illustrated in Fig. 4, through the combination of multi-view fusion and frequency-based regularization, our multi-prior score fusion method effectively addresses the theoretical limitations arising from the invalid conditional independence assumption in conventional approaches. By providing robust geometric structure and detailed texture guidance, we can mitigate artifacts caused by view correlations, resulting in synthesized images with improved coherence and fidelity across both visible and invisible regions.

3.4. Iterative Refinement Strategy

The iterative refinement strategy of our pipeline employs a systematic view rotation approach to progressively enhance

the 3DGS model. Starting from the initial angle Θ_0 of input views, we generate batches of rotated viewpoints at incremental angles $\Theta_1, \Theta_2, \dots$, gradually expanding coverage around the object (Fig. 5). For each batch of novel viewpoints, we generate high-quality, view-consistent images using our diffusion-based score fusion approach and use these images as supervision signals to refine the 3DGS model by optimizing Gaussian parameters with a composite loss function:

$$\mathcal{L}_{\text{total}} = \mathcal{L}_{\text{rec}} + \lambda \mathcal{L}_{\text{LPIPS}}, \quad (8)$$

where \mathcal{L}_{rec} measures pixel-wise reconstruction error and $\mathcal{L}_{\text{LPIPS}}$ computes the LPIPS loss using a pretrained VGG network [25]. During initial iterations, we densify the Gaussian representation by adding points in under-represented regions, followed by strategic pruning of low-opacity Gaussians to maintain computational efficiency. This rotated view sampling approach ensures progressive enhancement of both geometric and appearance details across the entire object, even in regions initially unobserved.

4. Experiments

4.1. Experimental Setup

We conduct extensive experiments on both synthetic and real-world datasets to evaluate the effectiveness of our approach. For synthetic evaluation, we utilize the Objaverse dataset [2], which provides ground truth images for quantitative assessment using SSIM [31], LPIPS [41] and PSNR metrics. Our real-world evaluation encompasses RefNeRF dataset and a custom dataset captured using an iPhone camera, where we employ the Segment Anything Model (SAM) [10] for background removal.

Our implementation builds on the Era3D [12] multi-view diffusion model as the MVD backbone and integrates Diff-BIR as the image restoration backbone. The diffusion process employs DDIM sampling with 50 steps. During refinement, we implement a progressive rotation strategy with controlled angular offsets in alternating directions to ensure comprehensive coverage. Each refinement iteration comprises 3,000 optimization steps for the Gaussian points, with densification applied during the initial 1,300 steps. To accommodate Era3D’s orthographic projection output, we adjust the rendering camera by increasing its distance by a factor of 100 and modifying the focal length accordingly. The hyper-parameters $\tau, \sigma, \eta, \Delta\theta, \delta_e$ and λ are set to 22, 7, 4, 45, 6, and 1, respectively.

4.2. Main Comparison

We compare our Zero-P-to-3 method against state-of-the-art approaches in both single-view and multi-view reconstruction categories. For a fair comparison, each method is adapted to our experimental setting: Zero-P-to-3 (Ours)

uses 90 images (30 each at $0^\circ, 30^\circ, -30^\circ$ elevation) covering 90° horizontally; GaussianObject [38] and Escher-Net [11] use 30 images at 0° elevation; Trellis [35] utilizes 5 images at $0^\circ, 30^\circ, 45^\circ, 60^\circ$, and 90° horizontal angles (all at 0° elevation); Era3D [12], LGM [27], and OpenLRM [7] each use a single image captured at 45° horizontal, 0° elevation; and 3DGS [9] uses the same 90 images as our method. This set of methods includes both reconstruction-based (3DGS, GaussianObject) and generative-based (Era3D, LGM, OpenLRM, Escher-Net, Trellis) techniques, enabling evaluation of different paradigms for 3D reconstruction from partial observations.

As illustrated in Table 1, our Zero-P-to-3 demonstrates superior performance on the Objaverse dataset across all evaluation metrics. Reconstruction-based methods like 3DGS achieve excellent fidelity in visible regions but struggle significantly with invisible regions. In contrast, generative methods such as Era3D and Trellis show more balanced performance between visible and invisible regions, though their overall metrics fall short of 3DGS due to the accuracy in visible regions of 3DGS. Our Zero-P-to-3 successfully combines the strengths of both paradigms, maintaining high fidelity in visible regions while generating consistent and realistic content in invisible regions. Qualitative evaluation in Fig. 6 further supports these findings, showing that our method produces more coherent geometric structures and preserves finer surface details. The areas highlighted in red boxes demonstrate where competing methods generate content that deviates significantly from ground truth, exhibiting inconsistencies with the input observations. Additional results are available in supplementary material.

4.3. Ablation Study

Analysis of Multi-view Fusion. As shown in Fig. 7, multi-view fusion significantly mitigates the issue of missing information from single-view inputs, greatly enhancing the quality and fidelity of the generated objects. This is particularly crucial in our setting, where observations are limited to partial views. These visual results align with the quantitative data presented in rows 1 and 2 of Table 2.

Analysis of Image Restoration Prior. The integration of the image restoration diffusion model also proves crucial for detail enhancement. The quality of the leftmost image in the second row of Fig. 8 (b) is the worst, which is because our rotation iteration strategy inevitably takes the rendering results of invisible views as the image condition for the input of MVD. However, the inference goal of MVD for the image is to restore the image condition as much as possible, which leads to the failure of the repair. The comparison results between Fig. 8 (a) and Fig. 8 (b) show that introducing the image restoration prior has solved this problem and can improve the repair quality in more invisible views. These

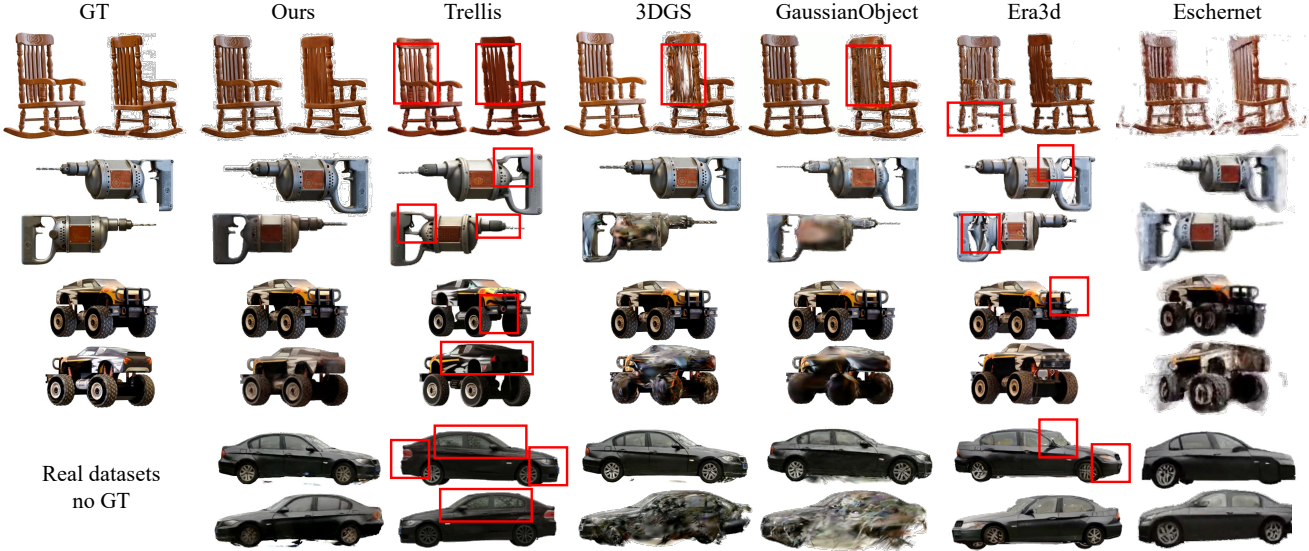


Figure 6. Qualitative comparisons between our method and other approaches. Reconstruction-based methods (3DGS, GaussianObject) achieve high fidelity in visible regions but struggle with invisible regions. In contrast, generative-based methods demonstrate the ability to synthesize reasonable geometric structures but often suffer from inconsistencies between generated content and observations (Trellis) or artifacts caused by generation inconsistencies (Era3D, EscherNet), particularly in the regions highlighted by red boxes. Our method successfully preserves details in visible regions while maintaining consistency across novel viewpoints. More qualitative results and comparisons are provided in the supplementary material.

Method	Visible Region			Invisible Region			Total Region		
	PSNR \uparrow	SSIM \uparrow	LPIPS \downarrow	PSNR \uparrow	SSIM \uparrow	LPIPS \downarrow	PSNR \uparrow	SSIM \uparrow	LPIPS \downarrow
3DGS	20.64	0.8958	0.0516	17.63	0.8319	0.1222	18.38	0.8479	0.1045
Era3d	16.23	0.8392	0.1312	15.60	0.8325	0.1399	15.76	0.8342	0.1377
LGM	12.58	0.7924	0.2078	12.34	0.7874	0.2179	12.40	0.7887	0.2154
LRM	13.84	0.8044	0.1896	12.56	0.8043	0.2098	12.88	0.8043	0.2048
EscherNet	18.68	0.8313	0.2275	15.61	0.7971	0.2636	16.38	0.8057	0.2546
GaussianObject	17.57	0.8535	0.0924	16.79	0.8360	0.1358	16.98	0.8403	0.1250
LGM (Era3d)	14.45	0.8145	0.1729	14.25	0.8154	0.1758	14.30	0.8152	0.1751
Trellis	16.68	0.8461	0.1121	16.31	0.8382	0.1188	16.40	0.8402	0.1172
Zero-P-to-3 (Ours)	20.53	0.8896	0.0604	18.14	0.8547	0.1016	18.74	0.8634	0.0913

Table 1. Quantitative comparison across different approaches. The table presents PSNR, SSIM, and LPIPS metrics for visible regions, invisible regions, and total reconstruction. Red numbers indicate best performance while pink indicates second best. 3DGS overfits to visible areas but performs poorly in invisible regions. Trellis demonstrates decent results in invisible areas but shows notable differences from ground truth. LGM (Era3D) represents results from replacing LGM’s backbone with Era3D. Our Zero-P-to-3 method achieves superior overall performance, effectively balancing fidelity in visible regions with consistent generation in invisible regions.

visual results align with the quantitative data presented in rows 7 and 8 of Table 2.

Analysis of Rendering Conditioned Inference. As described by Eq. (4) and Eq. (5), our Zero-P-to-3 incorporates the rendering results of 3DGS as the geometric prior for generating images. Figure 9 underscores the importance of our method. Without rendering guidance, generated results exhibit significant structural discrepancies from the original image. In contrast, Zero-P-to-3 produces images that maintain structural consistency and high-quality textures, ensuring effective object restoration. Quantitative results in Table

2 (rows 6 and 8) further support this improvement.

Analysis of Rotated View Sampling. Figure 10 reveals that the anisotropy of 3DGS [9] causes artifacts when repairing objects using only a few fixed viewing angles. This highlights the critical role of our rotated view sampling method, which densifies the supervision views, significantly enhancing rendering quality from novel perspectives and ensuring high-fidelity object reconstruction.

Analysis of Iterative Refinement Strategy. Fig. 11 clearly demonstrates how our iterative refinement strategy and fusion-based inference method work together to fundamen-

No.	Method	PSNR \uparrow	SSIM \uparrow	LPIPS \downarrow
Based on Era3D				
1	Era3D + NeuS	15.76	0.8432	0.1377
2	Era3D + MF + NeuS	16.06	0.8542	0.1310
Based on 3DGS				
3	3DGS	18.38	0.8479	0.1045
4	3DGS + MF	18.25	0.8559	0.0914
5	3DGS + MF + RVS	18.68	0.8615	0.0996
6	3DGS + MF + RVS + IRP	18.66	0.8579	0.0958
7	3DGS + MF + RVS + GP	18.38	0.8630	0.0921
8	Ours	18.74	0.8634	0.0913

Table 2. Ablation study on 3D scene reconstruction with diffusion models. Adding Multi-view Fusion(MF), Rotated View Sampling (RVS), Image Restoration Prior (IRP), and Geometric Prior (GP) enhances detail and quality, with Zero-P-to-3 combining all to achieve the best results, showing their combined strength.

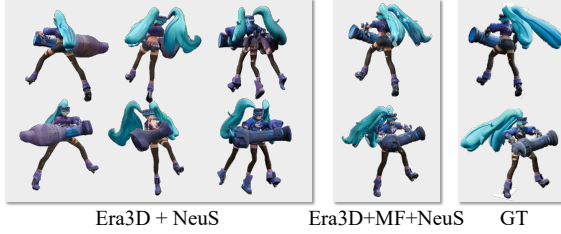


Figure 7. Ablation study on the effect of Multi-view Fusion (MF). The reconstruction using multi-view fusion with NeuS achieves high similarity to the ground truth (GT).

tally mitigate the issue caused by the conditional independence approximation. In traditional Multi-View Diffusion (MVD) inference, simply averaging the noisy predictions from different view conditions (as shown in Eq. (3)) can result in conflicts in regions where the information from the views does not overlap. For instance, in the sword region, different views give entirely different predictions, prevent-

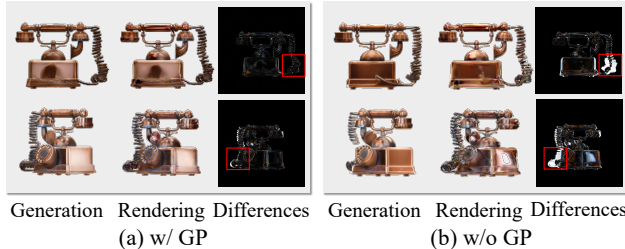


Figure 9. Effects of Geometric Prior in multi-view fusion. Each subplot presents diffusion-generated images, 3DGS-rendered images, and their differences. Red boxes in (b) (without Prior) indicate structural flaws, while (a) (with Prior) exhibits enhanced fidelity, highlighting the method’s importance.

ing consensus and leading to the area being treated as background noise and gradually eliminated.

To address this limitation, we introduce two comple-



Figure 8. Effects of applying the Image Restoration Prior (IRP) in multi-view fusion. The red boxes highlight notable quality differences, where images generated without the restoration prior exhibit degraded results compared to those with the prior enabled.



Figure 10. Effects of rotated view sampling. The regions framed in red show that there is a significant difference in texture quality between the two under specific viewing angles.

mentary priors in the multi-view fusion process. Low-frequency priors leverage initial geometric renderings to provide global structural constraints, effectively stabilizing the overall 3D layout. Simultaneously, high-frequency priors focus on recovering texture details, compensating for the blurring issues caused by the lack of correlation across multi-view information. These complementary priors to-



Figure 11. Analysis of direct reconstruction using results generated by Era3D. Yellow boxes highlight the failure to generate multi-view images of the sword, while red boxes indicate the failure of sword reconstruction. (a) shows the poor result after simply applying multi-view fusion, and this further leads to problems in (b).

gether resolve the issue of the invalid conditional independence assumption, enabling the iterative refinement process to utilize the original image’s rendered results to guide MVD sampling at each iteration, continuously improving the quality and 3D consistency of the generated images. Experimental results (see rows 2 and 8 in Table 2) confirm the effectiveness of this strategy in resolving conflicts and recovering missing details.

5. Conclusion

We present Zero-P-to-3, a novel training-free approach for high-quality 3D reconstruction from partial observations. Our method effectively addresses the challenges of partial-

view reconstruction through a pipeline that combines multi-view diffusion priors, image restoration, and iterative refinement with rotated view supervision. Experiments show its superior performance in both reconstruction quality and multi-view consistency. The Zero-P-to-3 framework’s success in handling incomplete observations opens doors to future work, including integration with other 3D representations and application to dynamic scenes.

References

- [1] David Charatan, Sizhe Li, Andrea Tagliasacchi, and Vincent Sitzmann. pixelsplat: 3d gaussian splats from image pairs for scalable generalizable 3d reconstruction, 2024. [1](#) [2](#)
- [2] Matt Deitke, Ruoshi Liu, Matthew Wallingford, Huong Ngo, Oscar Michel, Aditya Kusupati, Alan Fan, Christian Laforte, Vikram Voleti, Samir Yitzhak Gadre, Eli VanderBilt, Aniruddha Kembhavi, Carl Vondrick, Georgia Gkioxari, Kiana Ehsani, Ludwig Schmidt, and Ali Farhadi. Objaverse-xl: A universe of 10m+ 3d objects. *arXiv preprint arXiv:2307.05663*, 2023. [6](#)
- [3] Kangle Deng, Andrew Liu, Jun-Yan Zhu, and Deva Ramanan. Depth-supervised nerf: Fewer views and faster training for free. In *Proceedings of the IEEE/CVF Conference on Computer Vision and Pattern Recognition*, pages 12882–12891, 2022. [2](#)
- [4] Giuseppe Di Giacomo, Giulio Franzese, Tania Cerquitelli, Carla Fabiana Chiasserini, and Pietro Michiardi. Dimvis: Diffusion-based multi-view synthesis. In *ICML 2024 Workshop on Structured Probabilistic Inference {\&} Generative Modeling*, 2024. [3](#)
- [5] Liang Han, Junsheng Zhou, Yu-Shen Liu, and Zhizhong Han. Binocular-guided 3d gaussian splatting with view consistency for sparse view synthesis, 2024. [2](#)
- [6] Lukas Höllerin, Aljaž Božič, Norman Müller, David Novotny, Hung-Yu Tseng, Christian Richardt, Michael Zollhöfer, and Matthias Nießner. Viewdiff: 3d-consistent image generation with text-to-image models. In *Proceedings of the IEEE/CVF Conference on Computer Vision and Pattern Recognition*, pages 5043–5052, 2024. [3](#)
- [7] Yicong Hong, Kai Zhang, Juxiang Gu, Sai Bi, Yang Zhou, Difan Liu, Feng Liu, Kalyan Sunkavalli, Trung Bui, and Hao Tan. Lrm: Large reconstruction model for single image to 3d. *arXiv preprint arXiv:2311.04400*, 2023. [2](#) [6](#)
- [8] Hanwen Jiang, Zhenyu Jiang, Yue Zhao, and Qixing Huang. Leap: Liberate sparse-view 3d modeling from camera poses, 2023. [2](#)
- [9] Bernhard Kerbl, Georgios Kopanas, Thomas Leimkühler, and George Drettakis. 3d gaussian splatting for real-time radiance field rendering. *ACM Trans. Graph.*, 42(4):139–1, 2023. [2](#) [6](#) [7](#)
- [10] Alexander Kirillov, Eric Mintun, Nikhila Ravi, Hanzi Mao, Chloe Rolland, Laura Gustafson, Tete Xiao, Spencer Whitehead, Alexander C Berg, Wan-Yen Lo, et al. Segment anything. In *Proceedings of the IEEE/CVF International Conference on Computer Vision*, pages 4015–4026, 2023. [6](#)
- [11] Xin Kong, Shikun Liu, Xiaoyang Lyu, Marwan Taher, Xiaojuan Qi, and Andrew J. Davison. Eschneret: A generative model for scalable view synthesis, 2024. [2](#) [3](#) [6](#)
- [12] Peng Li, Yuan Liu, Xiaoxiao Long, Feihu Zhang, Cheng Lin, Mengfei Li, Xingqun Qi, Shanghang Zhang, Wenhan Luo, Ping Tan, et al. Era3d: High-resolution multiview diffusion using efficient row-wise attention. *arXiv preprint arXiv:2405.11616*, 2024. [1](#) [2](#) [3](#) [6](#)
- [13] Chen-Hsuan Lin, Jun Gao, Luming Tang, Towaki Takikawa, Xiaohui Zeng, Xun Huang, Karsten Kreis, Sanja Fidler, Ming-Yu Liu, and Tsung-Yi Lin. Magic3d: High-resolution text-to-3d content creation. In *Proceedings of the IEEE/CVF Conference on Computer Vision and Pattern Recognition*, pages 300–309, 2023. [3](#)
- [14] Fangfu Liu, Wenqiang Sun, Hanyang Wang, Yikai Wang, Haowen Sun, Junliang Ye, Jun Zhang, and Yueqi Duan. Reconx: Reconstruct any scene from sparse views with video diffusion model. *arXiv preprint arXiv:2408.16767*, 2024. [3](#)
- [15] Minghua Liu, Ruoxi Shi, Linghao Chen, Zhuoyang Zhang, Chao Xu, Xinyue Wei, Hansheng Chen, Chong Zeng, Jiayuan Gu, and Hao Su. One-2-3-45++: Fast single image to 3d objects with consistent multi-view generation and 3d diffusion. In *Proceedings of the IEEE/CVF Conference on Computer Vision and Pattern Recognition*, pages 10072–10083, 2024. [2](#)
- [16] Yuan Liu, Cheng Lin, Zijiao Zeng, Xiaoxiao Long, Lingjie Liu, Taku Komura, and Wenping Wang. Syncdreamer: Generating multiview-consistent images from a single-view image. *arXiv preprint arXiv:2309.03453*, 2023. [1](#) [3](#)
- [17] Xiaoxiao Long, Yuan-Chen Guo, Cheng Lin, Yuan Liu, Zhiyang Dou, Lingjie Liu, Yuexin Ma, Song-Hai Zhang, Marc Habermann, Christian Theobalt, et al. Wonder3d: Single image to 3d using cross-domain diffusion. In *Proceedings of the IEEE/CVF Conference on Computer Vision and Pattern Recognition*, pages 9970–9980, 2024. [1](#) [2](#) [3](#)
- [18] Michael Niemeyer, Jonathan T Barron, Ben Mildenhall, Mehdi SM Sajjadi, Andreas Geiger, and Noha Radwan. Regnerf: Regularizing neural radiance fields for view synthesis from sparse inputs. In *Proceedings of the IEEE/CVF Conference on Computer Vision and Pattern Recognition*, pages 5480–5490, 2022. [2](#)
- [19] Ben Poole, Ajay Jain, Jonathan T Barron, and Ben Mildenhall. Dreamfusion: Text-to-3d using 2d diffusion. *arXiv preprint arXiv:2209.14988*, 2022. [3](#)
- [20] Guocheng Qian, Jinjie Mai, Abdullah Hamdi, Jian Ren, Aliaksandr Siarohin, Bing Li, Hsin-Ying Lee, Ivan Skorokhodov, Peter Wonka, Sergey Tulyakov, et al. Magic123: One image to high-quality 3d object generation using both 2d and 3d diffusion priors. *arXiv preprint arXiv:2306.17843*, 2023. [3](#)
- [21] Robin Rombach, Andreas Blattmann, Dominik Lorenz, Patrick Esser, and Björn Ommer. High-resolution image synthesis with latent diffusion models, 2022. [1](#)
- [22] Johannes L Schonberger and Jan-Michael Frahm. Structure-from-motion revisited. In *Proceedings of the IEEE conference on computer vision and pattern recognition*, pages 4104–4113, 2016. [3](#)

[23] Ruoxi Shi, Hansheng Chen, Zhuoyang Zhang, Minghua Liu, Chao Xu, Xinyue Wei, Linghao Chen, Chong Zeng, and Hao Su. Zero123++: a single image to consistent multi-view diffusion base model. *arXiv preprint arXiv:2310.15110*, 2023. 3

[24] Yichun Shi, Peng Wang, Jianglong Ye, Mai Long, Kejie Li, and Xiao Yang. Mvdream: Multi-view diffusion for 3d generation. *arXiv preprint arXiv:2308.16512*, 2023. 2, 3

[25] Karen Simonyan and Andrew Zisserman. Very deep convolutional networks for large-scale image recognition. *arXiv preprint arXiv:1409.1556*, 2014. 6

[26] Stanislaw Szymanowicz, Christian Rupprecht, and Andrea Vedaldi. Splatter image: Ultra-fast single-view 3d reconstruction. In *Proceedings of the IEEE/CVF Conference on Computer Vision and Pattern Recognition*, pages 10208–10217, 2024. 3

[27] Jiaxiang Tang, Zhaoxi Chen, Xiaokang Chen, Tengfei Wang, Gang Zeng, and Ziwei Liu. Lgm: Large multi-view gaussian model for high-resolution 3d content creation. In *European Conference on Computer Vision*, pages 1–18. Springer, 2025. 2, 6

[28] Dor Verbin, Peter Hedman, Ben Mildenhall, Todd Zickler, Jonathan T Barron, and Pratul P Srinivasan. Ref-nerf: Structured view-dependent appearance for neural radiance fields. In *2022 IEEE/CVF Conference on Computer Vision and Pattern Recognition (CVPR)*, pages 5481–5490. IEEE, 2022. 3

[29] Vikram Voleti, Chun-Han Yao, Mark Boss, Adam Letts, David Pankratz, Dmitry Tochilkin, Christian Laforte, Robin Rombach, and Varun Jampani. Sv3d: Novel multi-view synthesis and 3d generation from a single image using latent video diffusion. In *European Conference on Computer Vision*, pages 439–457. Springer, 2025. 3

[30] Haochen Wang, Xiaodan Du, Jiahao Li, Raymond A Yeh, and Greg Shakhnarovich. Score jacobian chaining: Lifting pretrained 2d diffusion models for 3d generation. In *Proceedings of the IEEE/CVF Conference on Computer Vision and Pattern Recognition*, pages 12619–12629, 2023. 3

[31] Zhou Wang, Alan C Bovik, Hamid R Sheikh, and Eero P Simoncelli. Image quality assessment: from error visibility to structural similarity. *IEEE transactions on image processing*, 13(4):600–612, 2004. 6

[32] Kailu Wu, Fangfu Liu, Zhihan Cai, Runjie Yan, Hanyang Wang, Yating Hu, Yueqi Duan, and Kaisheng Ma. Unique3d: High-quality and efficient 3d mesh generation from a single image. *arXiv preprint arXiv:2405.20343*, 2024. 1, 2

[33] Rundi Wu, Ben Mildenhall, Philipp Henzler, Keunhong Park, Ruiqi Gao, Daniel Watson, Pratul P Srinivasan, Dor Verbin, Jonathan T Barron, Ben Poole, et al. Reconfusion: 3d reconstruction with diffusion priors. In *Proceedings of the IEEE/CVF Conference on Computer Vision and Pattern Recognition*, pages 21551–21561, 2024. 1, 2, 3

[34] Jamie Wynn and Daniyar Turmukhambetov. Diffusionerf: Regularizing neural radiance fields with denoising diffusion models. In *Proceedings of the IEEE/CVF Conference on Computer Vision and Pattern Recognition*, pages 4180–4189, 2023. 1, 2, 3

[35] Jianfeng Xiang, Zelong Lv, Sicheng Xu, Yu Deng, Ruicheng Wang, Bowen Zhang, Dong Chen, Xin Tong, and Jiaolong Yang. Structured 3d latents for scalable and versatile 3d generation, 2024. 2, 3, 6

[36] Jiale Xu, Weihao Cheng, Yiming Gao, Xintao Wang, Shenghua Gao, and Ying Shan. Instantmesh: Efficient 3d mesh generation from a single image with sparse-view large reconstruction models. *arXiv preprint arXiv:2404.07191*, 2024. 3

[37] Yinghao Xu, Zifan Shi, Wang Yifan, Hansheng Chen, Ceyuan Yang, Sida Peng, Yujun Shen, and Gordon Wetzstein. Grm: Large gaussian reconstruction model for efficient 3d reconstruction and generation. *arXiv preprint arXiv:2403.14621*, 2024. 2

[38] Chen Yang, Sikuang Li, Jiemin Fang, Ruofan Liang, Lingxi Xie, Xiaopeng Zhang, Wei Shen, and Qi Tian. Gaussianobject: Just taking four images to get a high-quality 3d object with gaussian splatting. *arXiv preprint arXiv:2402.10259*, 2024. 1, 2, 3, 6

[39] Hanyang Yu, Xiaoxiao Long, and Ping Tan. Lm-gaussian: Boost sparse-view 3d gaussian splatting with large model priors. *arXiv preprint arXiv:2409.03456*, 2024. 1, 2, 3

[40] Wangbo Yu, Jinbo Xing, Li Yuan, Wenbo Hu, Xiaoyu Li, Zhipeng Huang, Xiangjun Gao, Tien-Tsin Wong, Ying Shan, and Yonghong Tian. Viewcrafter: Taming video diffusion models for high-fidelity novel view synthesis. *arXiv preprint arXiv:2409.02048*, 2024. 3

[41] Richard Zhang, Phillip Isola, Alexei A Efros, Eli Shechtman, and Oliver Wang. The unreasonable effectiveness of deep features as a perceptual metric. In *Proceedings of the IEEE conference on computer vision and pattern recognition*, pages 586–595, 2018. 6

[42] Yingji Zhong, Lanqing Hong, Zhenguo Li, and Dan Xu. Cvt-xrf: Contrastive in-voxel transformer for 3d consistent radiance fields from sparse inputs. In *Proceedings of the IEEE/CVF Conference on Computer Vision and Pattern Recognition*, pages 21466–21475, 2024. 2

[43] Zi-Xin Zou, Zhipeng Yu, Yuan-Chen Guo, Yangguang Li, Ding Liang, Yan-Pei Cao, and Song-Hai Zhang. Triplane meets gaussian splatting: Fast and generalizable single-view 3d reconstruction with transformers. In *Proceedings of the IEEE/CVF Conference on Computer Vision and Pattern Recognition*, pages 10324–10335, 2024. 3